Geophys. J. Int. (2005) **161,** 829–838 doi: 10.1111/j.1365-246X.2005.02623.x

Lowermost mantle anisotropy beneath the north Pacific from differential *S–ScS* splitting

James Wookey,[1] J.-Michael Kendall[1] and Georg Rümpker[2]

[1] *School of Earth and Environment, University of Leeds, Woodhouse Lane, Leeds* LS2 9JT, *UK. E-mail: j.wookey@earth.leeds.ac.uk*
[2] *Fachbereich Geowissenschaften/Geographie, J. W. Goethe- Universität Frankfurt,* D-60323 *Frankfurt am Main, Germany*

Accepted 2005 March 3. Received 2005 February 24; in original form 2004 September 30

SUMMARY

Seismic anisotropy is an important tool for studying the nature, origin and dynamics of the lowermost mantle (D″). We introduce differential *S–ScS* splitting as a tool for removing the effect of near-source and near-receiver anisotropy to estimate splitting accrued in the D″ region. This is applicable to events recorded at epicentral distances between 60° and 85°. Near-source anisotropy has often been ignored in previous studies of lowermost mantle anisotropy. We apply differential *S–ScS* splitting to records from Canadian National Seismic Network stations of western Pacific earthquakes; these sample the lowermost mantle beneath the north Pacific. The residual splitting in *ScS*, which we attribute to D″, shows lag times between 1.0 and 3.9 s. Given the near horizontal ray path of *ScS* in D″, we interpret the recovered fast directions as the orientation of the fast shear wave in the plane defined by the vertical and transverse directions and observe a clearly non-VTI (transverse isotropy with a vertical axis of symmetry) style of anisotropy. The largest population of results shows an approximately southeasterly dipping symmetry axis which we speculate might be explained by descending palaeoslab material being swept horizontally across the core–mantle boundary towards an upwelling region beneath the central Pacific. Non-VTI symmetry and the many possible contributions to D″ anisotropy from lower-mantle minerals, melt and subducted materials suggest that our understanding of the lowermost mantle could be greatly improved by trying to resolve a more general style of anisotropy.

Key words: anisotropy, D″, lowermost mantle, shear wave splitting.

1 INTRODUCTION

The study of seismic anisotropy (the variation of seismic wave speed with direction) is an important tool in understanding dynamic processes in the Earth. Under favourable conditions it can provide a seismic signature to mantle flow invisible to other methods (such as tomography). Anisotropy in the mantle is observed most clearly near its boundaries, and its strongest expression is in the upper mantle (see reviews in Silver 1996; Montagner 1998; Savage 1999; Kendall 2000). There is also growing evidence for anisotropy in the transition zone and the uppermost lower mantle near the 660 km discontinuity, both globally (see, for example, Montagner & Kennett 1996; Trampert & Van Heijst 2002) and regionally (see, for example, Wookey *et al.* 2002; Chen & Brudzinski 2003; Wookey & Kendall 2004). Finally, there is a large body of evidence for significant anisotropy at the base of the mantle in the enigmatic D″ layer.

D″ is a region of anomalous velocity structure (see, for example, Masters *et al.* 2000; Ritsema & Van Heijst 2000) and exhibits—at varying depths—a seismic discontinuity in many regions (see, for example, Wysession *et al.* 1998; Thomas *et al.* 2002). There is also evidence for the presence of a thin (∼10 km) layer of ultra-low velocities at the base of the mantle in several regions (see Garnero *et al.* 1998 and references therein). D″ has been variously theorized to be a thermal or chemical boundary layer of subducted slab material or core–mantle interaction (see review in Wysession *et al.* 1998). Recently, it has been suggested that D″ is the site of a $MgSiO_3$ post-perovskite phase transformation (Murakami *et al.* 2004).

Anisotropy in D″ has been inferred in 1-D earth models by Montagner & Kennett (1996) and lateral coverage comes from the global model of Panning & Romanowicz (2004). Shear wave splitting in body wave phases has also been used extensively to study regional D″ anisotropy (see reviews in Lay *et al.* 1998; Kendall & Silver 1998; Moore *et al.* 2004). When a shear wave encounters an anisotropic medium, two orthogonal waveforms are generated, one propagating faster than the other. The two shear waves separate in time as they propagate. This delay and the polarization of the two waves persist after they have left the anisotropic medium and can be recorded at the surface. Phases commonly used for this analysis are *S*, *ScS* and *Sdiff* which propagate in the D″ region. In most studies the waveforms are examined for delays between the radial and transverse components (i.e. *SV* and *SH*), thus attempting to measure transverse isotropy with a vertical axis of symmetry (VTI;

also sometimes referred to as radial or polar anisotropy—see, for example, Thomsen 1986). If a more complex method is used (e.g. that of Silver & Chan 1991) non-vertical/horizontal fast directions, and hence more general forms of anisotropy, can be resolved.

One of the major challenges in these analyses is removing the effect of anisotropy near the source and receiver. The latter is commonly achieved using *SKS* results for the station as an estimate of the anisotropy in the upper mantle (e.g. Thomas & Kendall 2002). The influence of near-source anisotropy is less well constrained. Some studies simply neglect this factor altogether, others restrict their analysis to earthquakes below the olivine stability field (deeper than 410 km) (e.g. Thomas & Kendall 2002). This assumption, however, seems cast into doubt by recent evidence of anisotropy in the mid-mantle region (e.g. Wookey *et al.* 2002; Wookey & Kendall 2004). Other studies (e.g. Kendall & Silver 1996; Ritsema 2000) examine relative differences in phases from closer earthquakes which do not transit D″. This assumes no variation in source anisotropy between events which can be thousands of kilometres apart. Not accounting for source anisotropy is a serious potential flaw in many studies of D″ anisotropy to date (Lay *et al.* 1998). In this study, we apply a method for correcting for both source and receiver anisotropy to an example dataset from the Canadian National Seismic Network.

2 DATA AND METHODOLOGY

2.1 Data studied

We used eight events associated with subduction in the Western Pacific region recorded at Canadian National Seismic Network stations (see Tables 1 and 2). The events are associated with the subduction of the Pacific Plate beneath the Philippine Plate, south of the Pacific–Philippine–Eurasian triple-junction. This combination of events and stations gives *ScS* reflection points beneath the north Pacific (Fig. 1). These events and stations were previously used by Thomas *et al.* (2002) to map the D″ discontinuity. In total we looked at 371 source–receiver pairs.

2.2 *S–ScS* differential splitting

In order to address the problem of interference from anisotropy in the vicinity of the source and the receiver, we apply a three-layer splitting approach. This method is applicable to source–receiver pairs between $\Delta = 60^\circ$ and 85° epicentral distance. Example *S* and *ScS* ray paths for an event at 80° calculated for the reference model AK135 (Kennett *et al.* 1995) are given in Fig. 2, as is the receiver-side leg of *SKS* from an event 120° away. The *S* phase turns above D″ while the *ScS* wave samples it; both have similar paths in the upper mantle and transition zone. The lower mantle region above D″ is generally considered to be isotropic (see, for example, Montagner 1998; Kendall 2000, for reviews). With distances $>85^\circ$ the *S* phase begins to intersect the D″ discontinuity, and at distances $<60^\circ$ the ray paths become too separated.

Table 1. Table of events used in this study. Hypocentre locations and depths are from the ISC bulletin (ISC 2001). The source-side anisotropy Γ_S is measured by analysing *S* phases at stations DAWY, WALA and YKW1–3, and stacking the splitting results (Wolfe & Silver 1998). Events with no quoted δt or ϕ were identified as nulls. Errors are given by the 95 per cent confidence interval.

Date	Time	Lat.	Long.	Depth (km)	δt_{SRC}(s)	$\phi_{SRC}(^\circ)$
1995/10/01	1706	29.29	139.12	450 ± 2	—	—
1996/03/16	2204	28.96	138.98	482 ± 2	—	—
1996/06/09	0112	17.31	145.70	167 ± 4	0.8 ± 0.2	−13 ± 5
1996/07/15	1651	18.65	145.52	212 ± 6	0.7 ± 0.2	−2 ± 10
1999/01/12	0232	26.72	140.24	476 ± 3	—	—
1999/07/03	0530	26.29	140.56	450 ± 3	0.5 ± 0.2	30 ± 17
2000/10/27	0421	26.26	140.56	412 ± 4	1.0 ± 0.4	41 ± 17
2001/07/03	1310	21.63	142.98	325 ± 3	—	—

Table 2. Table of stations used in this study, and Γ_R corrections applied, either from *SKS* data (Evans *et al.* 2003), or from analysis of *S* splitting using the source-side corrections listed in Table 1. Errors are given by the 95 per cent confidence interval. Station PHC showed null splitting.

Station	Lat.	Long.	δt_{REC}(s)	$\phi_{REC}(^\circ)$	Source
DAWY	64.0	−139.3	1.4 ± 0.2	−58 ± 6	*SKS*
DLBC	58.4	−130.0	0.7 ± 0.2	6 ± 15	*S*
FNBC	58.8	−122.5	0.6 ± 0.2	24 ± 15	*S*
INK	68.3	−133.5	0.8 ± 0.6	78 ± 20	*S*
PHC	50.7	−127.4	—	—	*S*
PNT	49.3	−119.6	1.3 ± 0.2	72 ± 7	*S*
RES	74.6	−94.9	1.0 ± 0.2	−48 ± 9	*S*
WALA	49.0	−113.9	1.2 ± 0.1	60 ± 4	*SKS*
WHY	60.6	−134.8	1.1 ± 0.4	−46 ± 12	*S*
YKW1	62.4	−114.5	1.2 ± 0.2	44 ± 3	*SKS*
YKW2	62.4	−114.6	1.2 ± 0.2	49 ± 4	*SKS*
YKW3	62.5	−114.6	1.3 ± 0.1	45 ± 4	*SKS*

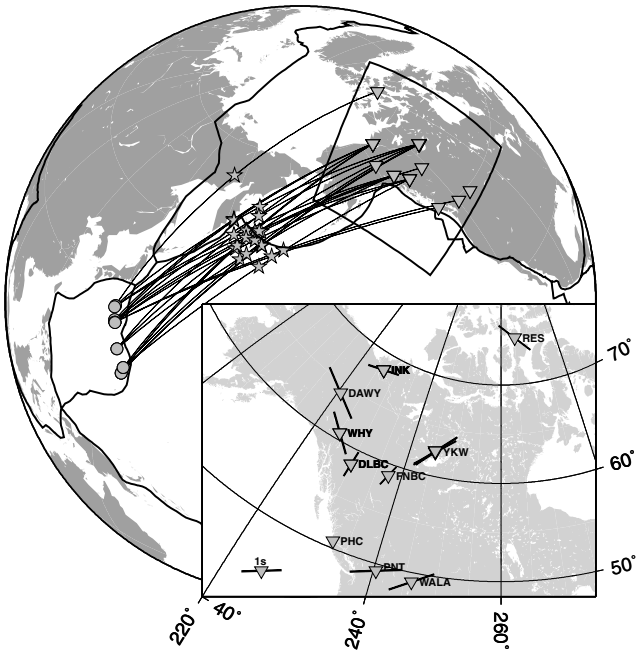

Figure 1. Map showing locations of events and stations used in this study, denoted by circles and triangles respectively. The events are associated with subduction in the western Pacific and the stations are part of the CNSN. Also shown are plate boundaries (thick lines), great circle ray paths (thin lines) and *ScS* reflection points (stars). The inset map shows the receiver-side shear wave splitting parameters determined for the stations. For the stations DAWY, WALA and YKW1–3 we use ISC reported *SKS* measurements (e.g. Evans *et al.* 2003), the remaining station corrections are determined from the *S* phases in our data. Black vectors indicate the fast direction, with length scaled by the lag time. These agree well with the orientations and magnitudes reported by Bostock & Cassidy (1995).

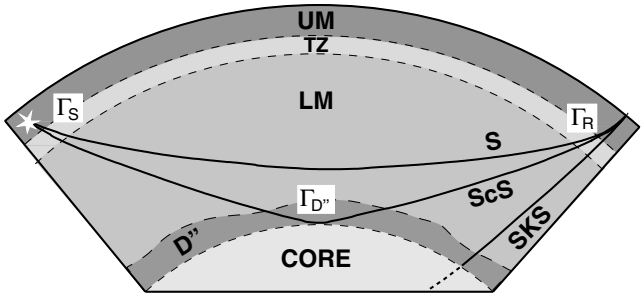

Figure 2. Ray paths for *S–ScS* differential splitting for a 150 km deep event recorded at 80° using the AK135 earth model (calculated using the TauP toolkit of Crotwell *et al.* 1999). The two phases have very similar paths in the transition zone and upper mantle; however, *ScS* samples D″ while *S* turns above it. Residual splitting in *ScS* after removal of *S* splitting is likely to be accrued in the lowermost mantle. Γ refers to the splitting operators in the source, receiver and D″ regions.

We analyse shear wave splitting in our data using the semiautomated method of Teanby *et al.* (2004) (an extension of the method of Silver & Chan 1991). This method attempts to minimize the effect of anisotropy on a pair of horizontal seismograms by correcting for a range of possible lag times (δt) and fast directions (ϕ), using a grid search. For each pair of values (each node on the grid) the eigenvalues of the covariance matrix of the two horizontal components are calculated. The best-fitting δt and ϕ correspond to the node with the smallest λ_2 (the smallest eigenvalue). These parameters best linearize the ellipticity of the particle motion. The error in the results is estimated by applying a statistical F-test, and using the extent of the 95 per cent confidence region. The method incorporates analysis window optimization based on cluster analysis (Teanby *et al.* 2004). We can also incorporate a source-side (Γ_S) and receiver-side (Γ_R) correction in our analysis. Γ_R is applied before the analysis; Γ_S is applied during the analysis to every node in the grid search to preserve the commutation of the splitting operators (see Wolfe & Silver 1998).

We first establish the receiver-side splitting operator Γ_R for the stations in the study. For the stations DAWY, WALA and YKW1–3 we use ISC reported *SKS* measurements (e.g. Evans *et al.* 2003). These stations have results covering the range of backazimuths appropriate to our data. They also show no significant variation in splitting parameters with backazimuth; thus we assume these results do not have a strong contribution from D″ anisotropy (Hall *et al.* 2004) or complex anisotropy beneath the stations (Silver & Savage 1994). Furthermore, they show good correlation with known crustal structural trends (Bostock & Cassidy 1995; Evans *et al.* 2003). We then use these results to establish the source-side splitting operator Γ_S for each event using the *S* phases in our data. This is done by measuring the splitting in the *S* wave at these stations after Γ_R correction (using the method outlined above). We assume that for the limited range of azimuths and slownesses in our data, the events will have a single Γ_S for all stations. This allows us to stack the splitting results using the method of Wolfe & Silver (1998) to get a high-quality estimate of Γ_S. These results are listed in Table 1. It is worth noting that half the events we looked at showed some source-side splitting. We then use these results to determine Γ_R for the stations without robust *SKS* data. This is done by correcting *S* phases in our data for Γ_S and analysing the residual splitting to estimate Γ_R. Again, we stack splitting results from several events to get a better estimate for each station. The stations and Γ_R measurements are listed in Table 2, and plotted in Fig. 1.

The shear wave splitting in the *ScS* phase is then analysed. The grid search is employed again over a range of possible δt and ϕ for Γ_D (the D″ shear wave splitting operator). For each node i in the grid the three shear wave splitting operators, Γ_R, $\Gamma_{D'',i}$ and Γ_S are removed in order (Γ_R and Γ_S are the fixed estimates determined from *S* and *SKS*) and the eigenvalues of the covariance matrix are determined. The node with the smallest post-correction λ_2 indicates the best-fitting splitting parameters for Γ_D. This residual splitting is most likely to be caused by anisotropy in D″. This method allows us to avoid restricting our dataset to events below 410 km, as we can estimate and remove a source term.

Splitting in *S* and *ScS* phases has been used previously to study D″ anisotropy in the central Pacific with a general fast-axis by Russell *et al.* (1998, 1999). However, these studies did not apply a source correction for events which showed measurable source anisotropy, but rather discarded them. Following a similar method with our dataset would have severely curtailed the number of results available. The source operator also provides useful information about anisotropy in the region of the event.

3 RESULTS

3.1 Source-side and receiver-side shear wave splitting

For the eight events in our dataset, four showed nulls and four showed measurable source-side splitting (Fig. 3). The splitting in these events is small (0.5–1 s), but does show an interesting pattern. The fast directions estimated are parallel to the descending slab. They are also compatible with the results of Fouch & Fischer (1996) to the north in the Izu-Bonin subduction zone, and suggest a rotation from a direction perpendicular to the absolute plate motion (APM) in the south to a more parallel direction to the north.

Many previous studies assume that events below 410 km will have no source-side anisotropy (as they are below the stability field of olivine) and for the most part our results are consistent with this assumption. Only one event significantly deeper than 410 km (19990703) shows evidence of source-side anisotropy, and this is a small amount. In fact, the events 19990112, 19990703 and

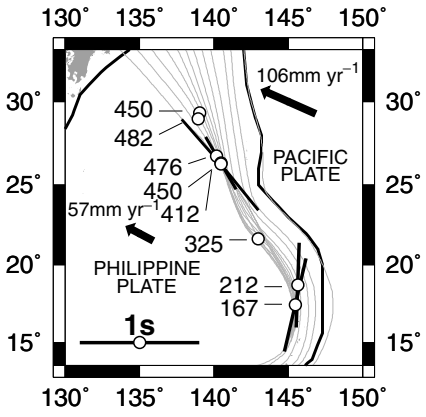

Figure 3. Source-side splitting parameters. The lag time δt and fast direction ϕ are plotted for the events used in the study, shown by open circles and annotated with hypocentre depth (km). The black line is the plate boundary, and grey contours are the depth of seismicity from Gudmundsson & Sambridge (1998). Vectors indicate the fast direction, with length scaled by the lag time; circles without vectors indicate nulls. The fast directions are convincingly slab-parallel. Also shown (arrows) are the absolute plate motion (APM) vectors for the Pacific and Philippine plates (Gripp & Gordon 1990).

20001027 show an interesting variation with depth. The hypocentres for these events are very close, and they show a decreasing anisotropy with depth (1 ± 0.4 s at 412 km, 0.5 ± 0.2 s at 450 km and null at 476 km). This is consistent with an anisotropic region which terminates at around 476 km. These results show that the technique we have outlined also produces useful information about anisotropy in the source region as well as the lowermost mantle. The small magnitude of the source-side splitting that we measure does suggest that correcting for it is not likely to have a large effect on our measurements of fast shear wave polarization (ϕ) direction in D″, since the effective two-layer splitting (Silver & Savage 1994) of Γ_S and $\Gamma_{D''}$ combined will be dominated by the greater anisotropy in the lowermost mantle. The source correction does, however, have a larger effect on the lag time δt than ϕ. For example, without source correction, event 1996/06/09 at YKW1 gives a result of $\delta t = 3.1 \pm 0.3$, $\phi = 60 \pm 20$ (compared with $\delta t = 2.7 \pm 0.1$, $\phi = 61 \pm 18$ after correction). In general, it is not valid to assume that source-side anisotropy will only have a small effect for other datasets where sources are located in different tectonic regions, especially if shallower sources are used.

The receiver corrections determined for the stations used are shown in Fig. 1 and Table 2. The magnitudes and directions determined are very similar to those reported by Bostock & Cassidy (1995). The orientations for northern stations correlate well with major tectonic features (the Tintina and Denali fault systems, and the Great Slave Lake shear zone). The three southern stations are oriented perpendicular to the Cascadia subduction zone, and may be related to subduction driven asthenospheric flow.

3.2 Lowermost mantle shear wave splitting

Of the 371 seismograms measured, 22 gave high-quality results for residual *ScS* splitting (Table 3). These are the results which had clearly identifiable *ScS* phases with a good signal-to-noise ratio, and gave well-constrained splitting solutions (i.e. convincingly linearized the particle motion). The errors on the results given are the 95 per cent confidence interval on the *ScS* analysis after correction of the best-fitting source and receiver parameters. This is likely to represent an underestimate of the error. To test this we ran the analysis for a single event (19960715 at DLBC) multiple times with the source and receiver corrections perturbed by their error estimates. This returned a range of $\phi = 38$–65 and $\delta t = 0.8$–1.6, compared with $\phi = 34$–54 and $\delta t = 0.7$–1.3 predicted by the 95 per cent confidence interval. Evidently, accounting for the uncertainty in the source and receiver corrections affects the final D″ estimate, but it appears that this effect is not very large. We have not extended this technique to the rest of the data, partially because of the small effect it has and also because it is unclear how to include null results in this analysis. To treat this problem in a more rigorous fashion would require a more involved error analysis in all splitting measurements, for example using a bootstrapping technique.

Fig. 4 shows an example analysis from the data. In this result, after the *S*-wave splitting parameters are removed, the residual splitting is measured as $\delta t = 2.7 \pm 0.3$ s, $\phi = -63 \pm 4°$. We attribute this splitting to anisotropy in D″. Although velocity heterogeneity in the lowermost mantle may distort a waveform from a simple linear polarization, such an effect would not give such clear shear wave splitting results, and so we believe that anisotropy is a much more likely mechanism to explain our results. Since the *ScS* ray path is close to horizontal in this region, we interpret ϕ in terms of the orientation of the fast shear wave in the plane defined by the vertical and transverse directions (i.e. backazimuth minus ϕ, which we denote ϕ^*). For normal *SKS* studies ϕ is the polarization azimuth of a vertically propagating fast shear wave. Fig. 5 shows further examples from the data set.

Fig. 6(a) shows the distribution of polarizations determined for the data. The average polarization in the data which dips east is 41 ± 7° (error is 95 per cent confidence interval); that is, a 41° dip from the horizontal plane. This is the dip of the projection of the fast direction onto the plane normal to the ray path. The most common style of anisotropy ascribed to the lowermost mantle is transverse isotropy with a vertical axis of symmetry (VTI), with $V_{SH} > V_{SV}$

Table 3. This table lists δt and ϕ for the residual *ScS* splitting ($\Gamma_{D''}$) measured in this study. Errors are given by the 95 per cent confidence interval. Anisotropy given assumes horizontal path in a 275 km thick D″ layer.

Event	Station	Δ(°)	$\Delta_{D''}$(°)	Backazimuth(°)	$\delta t_{D''}$(s)	$\phi_{D''}$(°)	Anisotropy (%)
1995/10/01	RES	70.5	19.5	311.5	1.3 ± 0.8	48 ± 6	0.82
1995/10/01	YKW3	71.4	20.0	297.8	3.9 ± 0.1	67 ± 5	2.32
1996/03/16	DLBC	66.3	17.5	286.9	1.5 ± 0.2	52 ± 9	1.05
1996/03/16	WHY	63.3	16.1	282.0	2.7 ± 0.2	63 ± 4	2.01
1996/06/09	INK	70.6	19.0	268.3	2.0 ± 0.2	54 ± 10	1.25
1996/06/09	YKW1	79.2	24.1	286.9	2.7 ± 0.1	61 ± 18	1.34
1996/06/09	YKW2	79.2	24.1	286.8	2.7 ± 0.1	70 ± 6	1.37
1996/06/09	YKW3	79.1	24.1	286.7	3.0 ± 0.5	63 ± 10	1.49
1996/07/15	DAWY	66.7	17.2	264.9	2.7 ± 0.2	−62 ± 4	1.89
1996/07/15	DLBC	71.3	19.5	275.3	1.0 ± 0.3	44 ± 10	0.66
1996/07/15	INK	69.3	18.4	268.7	2.6 ± 0.2	50 ± 5	1.69
1999/01/12	INK	64.1	16.3	277.2	1.0 ± 0.2	49 ± 18	0.72
1999/01/12	WHY	64.6	16.6	279.6	2.0 ± 0.1	49 ± 9	1.49
1999/07/03	DLBC	67.7	18.1	284.0	1.3 ± 0.2	−17 ± 8	0.89
1999/07/03	FNBC	71.3	20.0	289.8	1.3 ± 0.1	84 ± 11	0.82
1999/07/03	INK	64.3	16.4	276.7	1.1 ± 0.1	44 ± 8	0.81
1999/07/03	PHC	71.3	20.0	288.8	1.5 ± 0.3	23 ± 12	0.92
1999/07/03	PNT	76.5	23.1	294.6	1.4 ± 0.1	75 ± 5	0.74
2000/10/27	YKW3	73.5	21.1	295.2	3.3 ± 0.4	−49 ± 12	1.86
2001/07/03	INK	67.7	17.8	272.3	1.2 ± 0.3	48 ± 13	0.80
2001/07/03	WHY	67.5	17.7	274.3	1.8 ± 0.3	37 ± 6	1.26
2001/07/03	YKW3	76.5	22.7	290.9	2.9 ± 0.3	16 ± 7	1.53

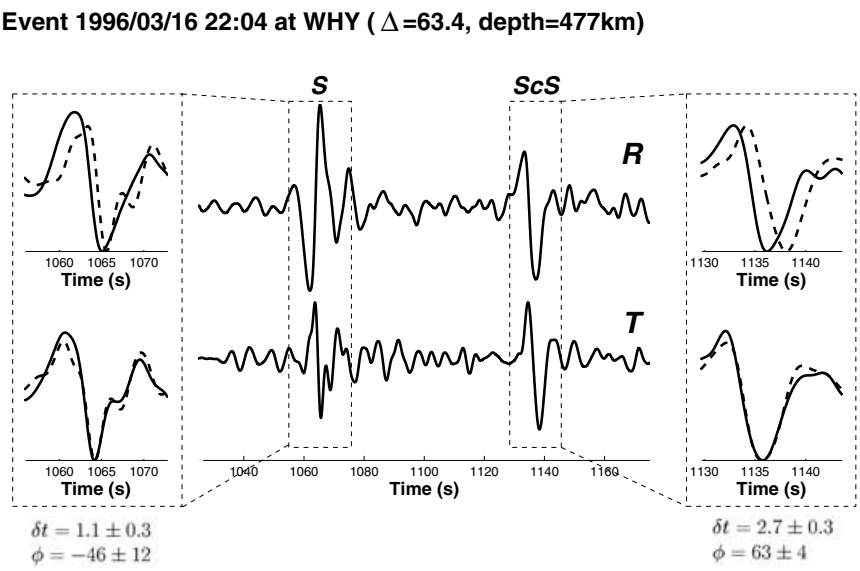

Figure 4. Example differential *S–ScS* splitting analysis of event 19960316 recorded at CNSN station WHY. Shown are the pre-analysis radial and transverse seismograms, filtered between 0.01 and 0.3 Hz to remove noise. The *S* and *ScS* phases are clearly identifiable. The inserts show the pre- and post-correction fast and slow shear waves for the *S* (left) and the residual *ScS* (right). In this case the splitting accrued in D″ is $\delta t = 2.7 \pm 0.3$ s.

in the symmetry plane (e.g. Lay *et al.* 1998; Kendall 2000; Moore *et al.* 2004; Panning & Romanowicz 2004). This would obviously show no apparent dip.

The simplest model that can explain our observations is anisotropy caused by the same mechanism, but with a tilted axis of symmetry (TTI). Assuming this style of anisotropy we can calculate the probability for a range of layer dips (see Appendix A and Fig. 8). This modelling demonstrates that the minimum possible dip is 41° and that dips greater than 65° cannot reproduce the average δt we observe (2 s). In turn, this limits the allowable range for the down-dip azimuth of the symmetry plane. Furthermore, the shallower dip models are compatible with our observed fast direction (41°) over a greater range of azimuths, making them more likely candidates. From this we can say that at the 95 per cent confidence level the layer dip is between 41° and 63° (and between 41° and 50° at the 66 per cent confidence level). This corresponds to a down-dip azimuth between 72° and 200° from north (or between 92° and 180° at the 66 per cent confidence level). The most likely model, therefore, is a layer dipping between 41° and 50° in a direction roughly south-east. To improve the constraint on this interpretation further would require detailed waveform modelling (e.g. Garnero *et al.* 2004), or imaging the region from a different azimuth. Of course, we cannot preclude the fact that the dipping fast-axis we resolve is the result of a more complex style of anisotropy, but our interpretation seems the most reasonable in the context of what has been observed in other regions of the lowermost mantle.

Fig. 6(b) shows the variation of the measured splitting time with event depth. The fact that there is no apparent trend is indicative of the success of the method at removing the influence of source anisotropy. The range of event depths used spans both the regions where strong anisotropy is likely (i.e. the upper 410 km of the mantle) and where anisotropy is probably much weaker (i.e. 520–660 km) (see, for example, Tommasi *et al.* 2004). The average splitting is 2.1 ± 0.4 s. To estimate the anisotropy this represents we assume that the splitting is accrued over a D″ layer of constant 275 km thickness (the average of the topography from Thomas *et al.* 2002), constant anisotropy and an average shear wave velocity from AK135 Kennett *et al.* (1995). We also approximate the *ScS* ray path as horizontal between entering and leaving this layer in order to calculate the distance travelled. This predicts that in order to reproduce the range of splitting observed requires 0.7–2.3 per cent anisotropy. This agrees well in general with previous observations (see review in Moore *et al.* 2004). Fig. 6(c) shows the variation of lag time (δt) with epicentral distance travelled in D″ ($\Delta_{D''}$). There is an indication of increasing δt with $\Delta_{D''}$, consistent with splitting accrued across a large area of weak anisotropy.

Fig. 7 shows the *ScS* shear wave splitting plotted at the predicted *ScS* bounce point. These are plotted as oriented discs (dark-shaded half indicates down-dip direction). Also plotted is the D″ discontinuity topography inferred by Thomas *et al.* (2002). The most prominent feature is a coherent band of results through most of the region, dipping roughly 40° towards the southeast. The topography on the reflector suggests that the region has complex structure and some scatter in the data is perhaps not surprising. We see no clear correlation between discontinuity topography and anisotropy dip.

4 DISCUSSION

The method we present is an iterative process for the quantification and removal of source- and receiver-side contributions to splitting observed in D″ using *ScS* phases. It has several advantages over simply using the deepest events and neglecting a source-side contribution. Firstly, it increases the number of candidate events available, indeed some source regions may not have any deep events. The estimation of the source anisotropy parameters is a useful resource in itself, and can be used to study, for example, subduction zone anisotropy in the region of the event. These source parameters can also be used to estimate receiver-side anisotropy in the upper mantle beneath stations where no or unreliable *SKS* data exist. The iterative nature of the process can be used to provide internal checks on results. The final result is an estimate of D″ anisotropy which has

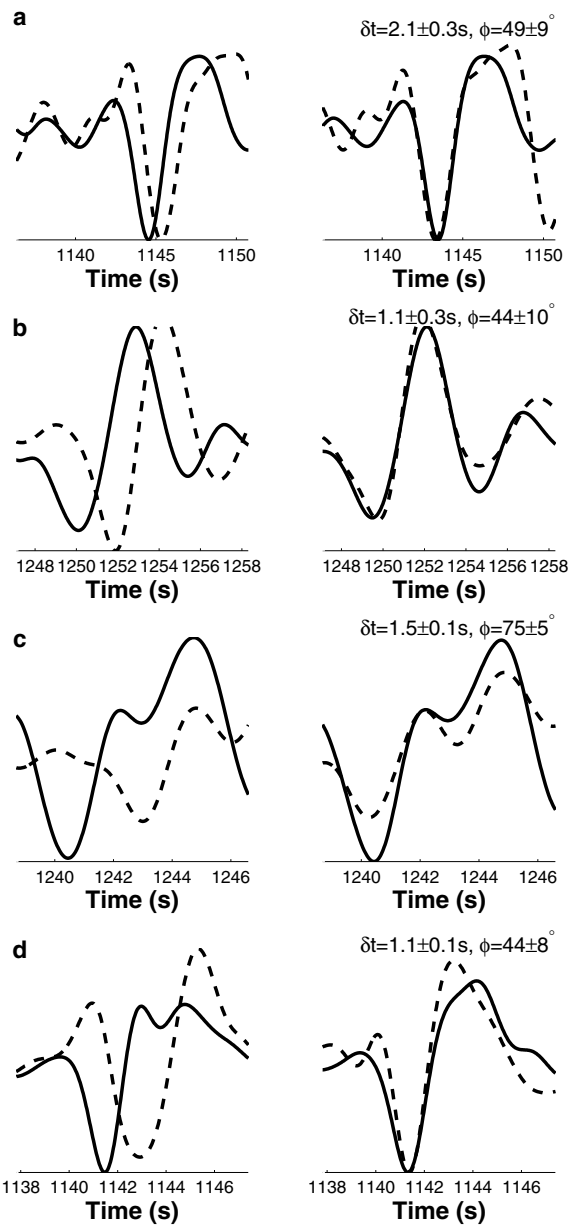

Figure 5. Further examples of residual *ScS* splitting from the data set. The pre- (left column) and post-analysis (right column) fast (solid line) and slow (dashed line) shear waves are shown. The results shown are: (a) event 1999/01/12 at WHY, (b) event 1996/07/15 at DLBC, (c) event 1999/07/03 at PNT and (d) event 1999/07/03 at INK.

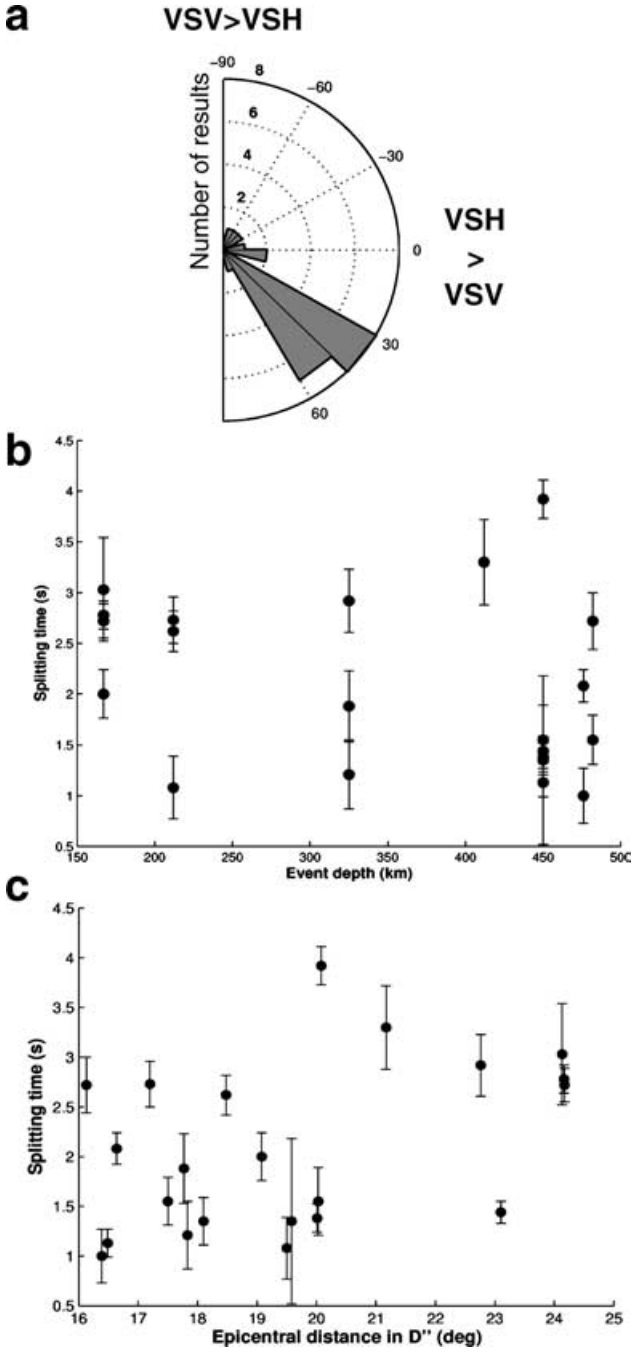

Figure 6. (a) Polar histogram of polarizations determined for residual *ScS* splitting. Due to the near-horizontal ray path in D″ these are interpreted as the orientation of the fast shear wave in the plane defined by the vertical and transverse directions (looking from source to receiver). The dominant population is a ∼40° dipping group. (b) Variation of residual *ScS* splitting lag time (δt) with event depth. There is no apparent relationship, suggesting that we are successfully removing the influence of near-source anisotropy. (c) The variation of splitting time with epicentral distance travelled in D″ (calculated assuming a 275 km thick D″ layer); this shows a rough positive correlation, consistent with splitting accrued across a large area of weak anisotropy.

had a robust 'ray path appropriate' correction for both source- and receiver-side contributions to the splitting.

Several studies of the lowermost mantle beneath Alaska (to the northeast of our study region) have looked for separation between the *SV* and *SH* components of various phases and have observed a general trend of $V_{SH} > V_{SV}$, with time lags of 0–5 s (e.g. Young & Lay 1990; Lay & Young 1991; Matzel *et al.* 1996; Garnero & Lay 1997; Wysession *et al.* 1999; Fouch *et al.* 2001). This is consistent with the long-wavelength trend shown by Panning & Romanowicz (2004). This has been attributed to the migration of palaeoslab material across the core–mantle boundary (CMB). Though it is unclear exactly how our dipping fast-axis results would map into a simple analysis of *SV*/*SH* separation, the averaged results of Garnero & Lay (1997) suggest that our region is isotropic. A 45° dipping fast axis might well distribute the fast shear wave pulse equally on the radial and transverse component, and thus display

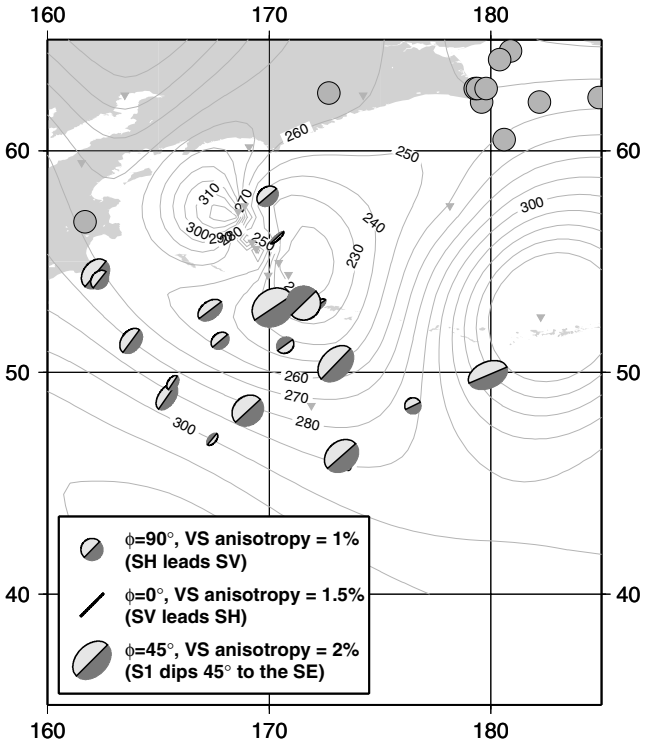

Figure 7. Map showing *ScS* splitting plotted at the reflection point. The results are shown as ellipses representing a plan view of an oriented disc (lower half shaded dark). The major axis of the ellipse is oriented with the ray direction, and is scaled based on the inferred D″ anisotropy. Also plotted is the inferred topography of the D″ reflector (in km) from Thomas *et al.* (2002) and locations where palaeosubducted slabs have been predicted to arrive at the CMB from Lithgow-Bertelloni & Richards (1998), denoted by grey circles.

no apparent *SV*/*SH* separation. Although we have a limited range of azimuths in our data, we have inferred that the most likely orientation of the anisotropy is a trend of dipping anisotropy towards the southeast. The area which we image has been associated with the site where palaeoslabs are predicted to have impinged on the CMB (Lithgow-Bertelloni & Richards 1998). If the anisotropy we observe is caused by the alignment of subducted material, or is aligned by strain associated with subduction (e.g. McNamara *et al.* 2001), we speculate that a dipping fast-axis may result when vertically descending material is swept horizontally along the CMB. This horizontal flow is likely to be towards regions associated with upwelling, for example beneath the central Pacific (e.g. Panning & Romanowicz 2004), which lies roughly to the southeast of our study area. This is compatible with previous explanations postulated for lowermost mantle anisotropy beneath Alaska (e.g. Wysession *et al.* 1999; Fouch *et al.* 2001).

Lowermost mantle anisotropy beneath the Caribbean has also been studied extensively (e.g. Mitchell & Helmberger 1973; Kendall & Silver 1996; Garnero *et al.* 2004). This is an apparently similar dynamic situation as beneath the north Pacific as it is also associated with palaeoslab material arriving the CMB (e.g. Lithgow-Bertelloni & Richards 1998; Kendall & Silver 1998). These studies predominantly used *SV*/*SH* separation, and show a general pattern of *SH* leading *SV* similar to beneath Alaska. Recent work, however, by Garnero *et al.* (2004) has also attempted to resolve TTI-style anisotropy using waveform modelling. This study shows scattered small (∼20°) dips east and west, and also some results compatible with VTI-style anisotropy.

Beneath the central Pacific, the pattern of lowermost mantle anisotropy appears more complicated, with both $V_{SH} > V_{SV}$ and $V_{SV} > V_{SH}$ inferred from different studies (e.g. Pulliam & Sen 1998; Vinnik *et al.* 1998; Fouch *et al.* 2001). Russell *et al.* (1998, 1999) have also studied more general anisotropy, and found a scatter of non-radial/transverse fast directions. These seem to suggest a rotation of fast direction over a short distance which the authors attribute to local flow patterns associated with the upwelling of a large Hawaiian plume. It is possible that the variability in the previous results for this region might be associated with smooth spatial variation of the dip of the anisotropic symmetry axis.

Several explanations for D″ anisotropy have been suggested. Firstly, the anisotropy could be due to the lattice-preferred orientation (LPO) of $MgSiO_3$ in perovskite (e.g. Kendall & Silver 1998; Stackhouse *et al.* 2005) or post-perovskite (Tsuchiya *et al.* 2004; Stackhouse *et al.* 2005) forms, or the alignment of MgO (Karato 1998; Karki *et al.* 1999). Recent work by Stackhouse *et al.* (2005) has shown that post-perovskite can explain a horizontal fast shear wave at lower mantle pressures and temperatures. This makes it an excellent candidate for explaining anisotropy in the colder regions of the lowermost mantle (e.g. beneath the Caribbean and north Pacific) associated with descending slab material. However, the phase boundary calculated for post-perovskite probably precludes it being present in sufficient quantity in hotter regions (Oganov & Ono 2004) such as the central Pacific. Another issue is the dislocation creep style deformation required to produce LPO. This has been observed in perovskite experimentally under uppermost lower-mantle pressure and temperature conditions (Cordier *et al.* 2004), but post-perovskite has not yet been studied. Nevertheless, an LPO of post-perovskite aligned by flow associated with subduction presents a compelling explanation for the results we observe.

Alternatively, the anisotropy could be explained by the shape-preferred orientation (SPO) of inclusions of subducted materials or melt (Kendall & Silver 1996, 1998). These can display a strong anisotropic signature, even for very small volume fractions of included materials (Kendall & Silver 1996; Moore *et al.* 2004). Candidate inclusion materials include molten remnant subducted basalts (Hirose *et al.* 1999) and iron from the core (e.g. Wysession *et al.* 1998).

One or more of these types of anisotropy could be contributing to the observed signature. Differentiating between them, and making inferences about flow and deformation in D″, is a significant challenge. Attempting to resolve a more general form of anisotropy is a step towards this: for example, it potentially allows us to map flow in the lowermost mantle in three dimensions. Methods which estimate a more general style of anisotropy require careful treatment of the contributions from near-source and receiver anisotropy. This will also to allow us to extend the coverage of the lowermost mantle and make more robust regional comparisons.

ACKNOWLEDGMENTS

The authors would like to thank Matt Evans at the ISC for providing the *SKS* results and the CNSN for providing the data. We also thank the members of the Deep Earth System consortium, Tine Thomas, Thorsten Becker, Matt Fouch and an anonymous reviewer for their useful comments on the manuscript. This work was supported by NERC consortium grant O/2001/00668.

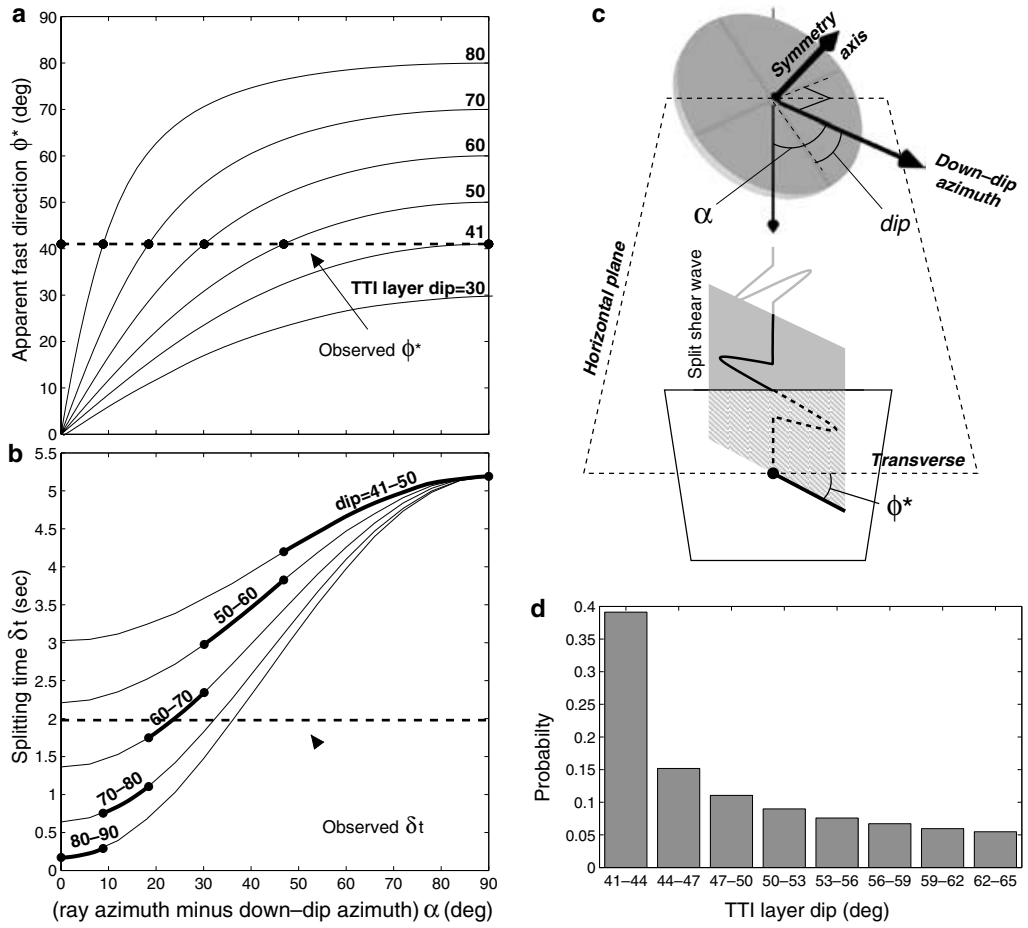

Figure 8. Predicted shear wave fast direction and splitting time for a transversely isotropic medium with a tilted axis of symmetry. These graphs show the variation of apparent fast-axis ϕ^* (a) and splitting time δt (b) with azimuth of wave propagation from the down-dip direction (denoted α) in a TTI model with various degrees of dip. Both of these graphs are symmetrical about 90° azimuth. On each panel the heavy dashed line shows the average parameters observed in our data. The circles denote the azimuths at which the average apparent fast direction matches our observation for each dip. These circles therefore bracket the range of azimuths allowed for intermediate dips. For example, a layer dipping between 41° and 50° can only be observed between azimuths of 47° and 90°. These define the maximum observable splitting time in (b) (bold sections of curves). This allows us to exclude dips greater than 65° as they display <2 s of splitting, and thus reduce the range of possible azimuths. Based on the proportion of the allowable azimuth range covered by each range of dips we can calculate a probability distribution for model dip (d). This shows that the shallowest allowed dips are the most likely: 41°–62° at the 95 per cent confidence level, and 41°–50° at the 66 per cent level.

REFERENCES

Bostock, M.G. & Cassidy, J.F., 1995. Variations in SKS splitting across western Canada, *Geophys. Res. Lett.,* **22,** 5–8.

Chen, W.-P. & Brudzinski, M.R., 2003. Seismic anisotropy in the mantle transition zone beneath Fiji-Tonga, *Geophys. Res. Lett.,* **30,** 1682.

Cordier, P., Ungáar, T., Zsoldos, L. & Tichy, G., 2004. Dislocation creep in $MgSiO_3$, *Nature,* **428,** 837–840.

Crotwell, H.P., Owens, T.J. & Ritsema, J., 1999. The TauP toolkit; flexible seismic travel-time and ray-path utilities, *Seism. Res. Lett.,* **70,** 154–160.

Evans, M.S., Kendall, J.-M. & Willemann, R.J., 2003. Development of automated SKS splitting measurement—an additional parameter to be provided by the ISC, *EOS, Trans. Am. geophys. Un.,* **84,** Abstract S32C–03

Fouch, M.J. & Fischer, K.M., 1996. Mantle anisotropy beneath northwest Pacific subduction zones, *J. geophys. Res.,* **101,** 15 987–16 002.

Fouch, M.J., Fischer, K.M. & Wysession, M.E., 2001. Lowermost mantle anisotropy beneath the Pacific; imaging the source of the Hawaiian plume, *Earth planet. Sci. Lett.,* **190,** 167–180.

Garnero, E. & Lay, T., 1997. Lateral variations mantle shear wave anisotropy beneath the north Pacific and Alaska, *J. geophys. Res.,* **102,** 8121–8135.

Garnero, E.J., Revenaugh, J., Lay, T. & Kellog, L., 1998. Ultralow velocity zone at the core-mantle boundary, in *The Core–Mantle Boundary Region, American Geophysical Union Geodynamics Series 28*, pp. 319–334, eds Gurnis, M., Wysession, M.E., Knittle, E. & Buffett, B.A., American Geophysical Union, Washington, DC.

Garnero, E.J., Maupin, V., Lay, T. & Fouch, M.J., 2004. Variable azimuthal anisotropy in Earth's lowermost mantle, *Science,* **306,** 259–261.

Gripp, A.E. & Gordon, R.G., 1990. Current plate velocities relative to the hotspots incorporating the NUVEL-1 global plate motion model, *Geophys. Res. Lett.,* **17,** 1109–1112.

Gudmundsson, O. & Sambridge, M., 1998. A regionalised upper mantle (RUM) seismic model, *J. geophys. Res.,* **103,** 7121–7136.

Hall, S.A., Kendall, J.-M. & der Baan, M.V., 2004. Some comments on the effects of lower-mantle anisotropy on SKS and SKKS phases, *Phys. Earth planet. Int.,* **146,** 469–481.

Hirose, K., Fei, Y., Ma, Y. & Mao, H.-K., 1999. The fate of subducted basaltic crust in the Earth's lower mantle, *Nature,* **397,** 53–56.

International Seismological Centre, 2001. On-line bulletin (http://www.isc.ac.uk/Bull).

Karato, S., 1998. Some remarks on the origin of seismic anisotropy in the D″ layer, *Earth Planets Space,* **50,** 1019–1028.

Karki, B.B., Wentzcovitch, R.M., de Gironcoli, S. & Baroni, S., 1999. First-principles determination of elastic anisotropy and wave velocities of MgO at lower mantle conditions, *Science,* **286,** 1705–1707.

Kendall, J.-M., 2000. Seismic anisotropy in the boundary layers of the mantle, in *Earth's Deep Interior: Mineral physics and Tomography From the Atomic to the Global Scale,* American Geophysical Union Geophysical Monograph 117, pp. 133–159, eds Karato, S., Forte, A., Liebermann, R., Masters, G. & Stixrude, L., American Geophysical Union, Washington, DC.

Kendall, J.-M. & Silver, P.G., 1996. Constraints from seismic anisotropy on the nature of the lower mantle, *Nature,* **381,** 409–412.

Kendall, J.-M. & Silver, P.G., 1998. Investigating causes of D″ anisotropy, in *The Core–Mantle Boundary Region,* American Geophysical Union Geodynamics Series 28, pp. 97–118, eds Gurnis, M., Wysession, M.E., Knittle, E. & Buffett, B.A., American Geophysical Union, Washington, DC.

Kennett, B. L.N., Engdahl, E.R. & Buland, R., 1995. Constraints on seismic velocities in the Earth from traveltimes, *Geophys. J. Int.,* **122,** 108–124.

Lay, T. & Young, C.J., 1991. Analysis of seismic SV-waves in the core's penumbra, *Geophys. Res. Lett.,* **18,** 1373–1376.

Lay, T., Williams, Q., Garnero, E.J., Kellogg, L. & Wysession, M.E., 1998. Seismic wave anisotropy in the D″ region and its implications, in *The Core–Mantle Boundary Region,* American Geophysical Union Geodynamics Series 28, pp. 299–318, eds Gurnis, M., Wysession, M.E., Knittle, E. & Buffett, B.A., American Geophysical Union, Washington, DC.

Lithgow-Bertelloni, C. & Richards, M.A., 1998. The dynamics of Cenozoic and Mesozoic plate motions, *Rev. Geophys.,* **36,** 27–78.

Masters, G., Laske, G., Bolton, H. & Dziewonski, A.M., 2000. The relative behaviour of shear velocity, bulk sound speed, and compressional velocity in the mantle: implications for chemical and thermal structure, in *Earth's Deep Interior: Mineral Physics and Tomography From the Atomic to the Global Scale,* American Geophysical Union Geophysical Monograph 117, pp. 201–213, eds Karato, S., Forte, A., Liebermann, R., Masters, G. & Stixrude, L., American Geophysical Union, Washington, DC.

Matzel, E., Sen, M.K. & Grand, S.P., 1996. Evidence for anisotropy in the deep mantle beneath Alaska, *Geophys. Res. Lett.,* **23,** 2417–2420.

McNamara, A.K., Karato, S. & Van Keken, P.E., 2001. Localization of dislocation creep in the lower mantle: implications for the origin of seismic anisotropy, *Earth planet. Sci. Lett.,* **191,** 85–99.

Mitchell, B.J. & Helmberger, D.V., 1973. Shear velocities at the base of the mantle from observations of S and ScS, *J. geophys. Res.,* **78,** 6009–6020.

Montagner, J.-P., 1998. Where can seismic anisotropy be detected in the Earth's mantle? In boundary layers . . . , *Pure appl. Geophys.,* **151,** 223–256.

Montagner, J.-P. & Kennett, B. L.N., 1996. How to reconcile body-wave and normal-mode reference Earth models, *Geophys. J. Int.,* **125,** 229–248.

Moore, M.M., Garnero, E.J., Lay, T. & Williams, Q., 2004. Shear wave splitting and waveform complexity for lowermost mantle structures with low-velocity lamellae and transverse isotropy, *J. geophys. Res.,* **109,** B02319, doi:10.1029/2003JB002546.

Murakami, M., Hirose, K., Kawamura, K., Sata, N. & Ohishi, Y., 2004. Post-perovskite phase transition in MgSiO3, *Science,* **304,** 855–857.

Oganov, A.R. & Ono, S., 2004. Theoretical and experimental evidence for a post-perovskite phase of MgSiO3 in Earth's D″ layer, *Nature,* **430,** 445–448.

Panning, M. & Romanowicz, B., 2004. Inferences on flow at the base of Earth's mantle based on seismic anisotropy, *Science,* **303,** 351–353.

Pulliam, J. & Sen, M.K., 1998. Seismic anisotropy in the core–mantle transition zone, *Geophys. J. Int.,* **135,** 113–128.

Ritsema, J., 2000. Evidence for shear velocity anisotropy in the lowermost mantle beneath the Indian Ocean, *Geophys. Res. Lett.,* **27,** 1041–1044.

Ritsema, J. & Van Heijst, H.J., 2000. Seismic imaging of structural heterogeneity in Earth's mantle: evidence for large-scale mantle flow, *Sci. Progr.,* **83,** 243–259.

Russell, S., Lay, T. & Garnero, E.J., 1998. Seismic evidence for small-scale dynamics in the lowermost mantle at the root of the Hawaiian hotspot, *Nature,* **396,** 255–258.

Russell, S., Lay, T. & Garnero, E.J., 1999. Small-scale lateral shear velocity and anisotropy heterogeneity near the core–mantle boundary beneath the central Pacific imaged using broadband ScS waves, *J. geophys. Res.,* **104,** 13 183–13 199.

Savage, M.K., 1999. Seismic anisotropy and mantle deformation: what have we learned from shear wave splitting?, *Rev. Geophys.,* **37,** 65–106.

Silver, P.G., 1996. Seismic anisotropy beneath the continents: probing the depths of geology, *Annu. Rev. Earth planet. Sci.,* **24,** 385–432.

Silver, P.G. & Chan, W.W.J., 1991. Shear-wave splitting and subcontinental mantle deformation, *J. geophys. Res.,* **96,** 16 429–16 454.

Silver, P. & Savage, M.K., 1994. The interpretation of shear-wave splitting parameters in the presence of 2 anisotropic layers, *Geophys. J. Int.,* **119,** 949–963.

Stackhouse, S., Brodholt, J.P., Price, G.D., Wookey, J. & Kendall, J.-M., 2005. The effect of temperature on the acoustic anisotropy of the perovskite and post-perovskite polymorphs of MgSiO3, *Earth planet. Sci. Lett.,* **230,** 1–10.

Teanby, N.A., Kendall, J.-M. & Van der Baan, M., 2004. Automation of shear-wave splitting measurements using cluster analysis, *Bull. seism. Soc. Am.,* **94,** 453–463.

Thomas, C. & Kendall, J.-M., 2002. The lowermost mantle beneath northern Asia—II. Evidence for lower-mantle anisotropy, *Geophys. J. Int.,* **151,** 296–308.

Thomas, C., Heesom, T. & Kendall, J.-M., 2002. Investigating the heterogeneity of the D″ region beneath the northern Pacific using a seismic array, *J. geophys. Res.,* **107**. B002274, doi:10.1029/2000JB000021.

Thomsen, L., 1986. Weak elastic anisotropy, *Geophysics,* **51,** 1954–1966.

Tommasi, A., Mainprice, D., Cordier, P., Thoraval, C. & Couvy, H., 2004. Strain-induced seismic anisotropy of wadsleyite polycrystals: constraints on flow patterns in the mantle transition zone, *J. geophys. Res.,* B12405, doi:10.1029/2004JB003158.

Trampert, J. & Van Heijst, H.J., 2002. Global azimuthal anisotropy in the transition zone, *Science,* **296,** 1297–1299.

Tsuchiya, T., Tsuchiya, J., Umemoto, K. & Wentzcovitch, R.M., 2004. Elasticity of post-perovskite MgSiO3,, *Geophys. Res. Lett.,* **31,** L14603, doi:10.1029/2004GL020278.

Vinnik, L.P.R., Breger, L. & Romanowicz, B., 1998. Anisotropic structures at the base of the Earth's mantle, *Nature,* **393,** 564–567.

Wolfe, C.J. & Silver, P.G., 1998. Seismic anisotropy of oceanic upper mantle: shear wave splitting methodologies and observations, *J. geophys. Res.,* **103,** 749–771.

Wookey, J. & Kendall, J.-M., 2004. Evidence of mid-mantle anisotropy from shear wave splitting and the influence of shear-coupled P waves, *J. geophys. Res.,* **109,** B07309, doi:10.1029/2003JB002871.

Wookey, J., Kendall, J.-M. & Barruol, G., 2002. Mid-mantle deformation inferred from seismic anisotropy, *Nature,* **415,** 777–780.

Wysession, M.E., Lay, T., Revenaugh, J., Williams, Q., Garnero, E.J., Jeanloz, R. & Kellog, L.H., 1998. The D″ discontinuity and its implications, in *The Core–Mantle Boundary Region,* American Geophysical Union Geodynamics Series 28, pp. 97–118, eds Gurnis, M., Wysession, M.E., Knittle, E. & Buffett, B.A., American Geophysical Union, Washington, DC.

Wysession, M.E., Langenhorst, A., Fouch, M.J., Fischer, K.M., Al-Eqabi, G.I., Shore, P.J. & Clarke, T.J., 1999. Lateral variations in compressional/shear velocities at the base of the mantle, *Science,* **284,** 120–125.

Young, C.J. & Lay, T., 1990. Multiple phase analysis of the shear velocity structure in the D″ region beneath Alaska, *J. geophys. Res.,* **95,** 17 385–17 402.

APPENDIX A: INTERPRETATION OF FAST DIRECTION

The fast shear wave polarization we determine from our data clearly deviates from the simple vertical transverse isotropy (VTI) style of anisotropy most commonly ascribed to the lowermost mantle (e.g. Lay *et al.* 1998; Kendall 2000; Moore *et al.* 2004; Panning & Romanowicz 2004). The simplest model to explain our data is one

invoking the same style of anisotropy, but with the symmetry axis tilted from the vertical (TTI), as might be observed with a dipping layer. We can interpret the fast direction we recover in terms of the dip and down-dip azimuth of the symmetry plane of such a medium. Although we cannot exactly determine these parameters without data from multiple azimuths, we can make a 'most-likely' model argument. For a given TTI model (assuming lowermost mantle velocities from AK135) we can calculate an 81-component stiffness C_{ijkl} matrix. We can then determine the velocity and polarization of the two shear waves for any given direction of propagation by solving the Christoffel equation:

$$\left(C_{ijkl}X_iX_j - \delta_{kl}\rho v^2\right)U_k = 0, \tag{A1}$$

where X_i and X_j define the wave front normal, ρ is the density, v is the phase velocity, δ_{kl} is the Kronecker delta function and U_k are the amplitudes ($i, j, k, l = 1$–3, the principal Cartesian axes). This allows us to predict the fast direction and splitting time we would observe for a TTI model with a shear phase horizontally traversing the medium at a given azimuth (i.e. angle from the down-dip direction, α in Fig. 8c). Fig. 8 shows the comparison of this modelling with the average fast direction and splitting time observed for our data. To generate these models we have a assumed 4 per cent anisotropy, which we consider to be a reasonable maximum to exist over a large distance in the lowermost mantle (e.g. Kendall 2000). Figs 8a and b show these parameters calculated for a range of dips, assuming a 1000 km path in D″ ($\sim$65° epicentral distance). Also shown as a heavy dashed line are the average fast directions and split times for the data. This shows that to observe a 41° apparent fast direction (ϕ^*) requires a 41° or steeper dip. In Fig. 8a the intersections of the different dip curves and the dashed line define the azimuth of propagation at which a TTI layer with such a dip would give a 41° apparent fast direction. Therefore, the gaps between these points represent the range of azimuths possible for a range of dips, for example, a layer dipping between $\alpha = 41°$ and 50° must be being observed between 47° and 90°. These distances have been translated to Fig. 8b (the heavy section on each curve). These sections represent the maximum splitting which may be observed for a given range of dips that is compatible with the observed fast direction. From this we determine that dips of 65° and greater do not produce enough splitting to match our observation; this, in turn, limits the range of possible azimuths. We can use these factors to produce a probability distribution for a range of layer dips (Fig. 8d). This is simply the range of azimuths for which we can expect to observe a given dip range divided by the total possible range of azimuths (after excluding that occupied by dips of 65° or greater). The shallowest dips are the most likely: 41°–62° at the 95 per cent confidence level and 41°–50° at the 66 per cent level. These correspond to azimuths between 28° and 90° and 47° and 90° respectively. These can be either clockwise or anticlockwise from the down-dip azimuth. It should be explained that this is the most optimistically broad range of allowable dips as we have assumed a large amount of anisotropy (4 per cent). Smaller amounts would further restrict the range of allowable dips and down-dip azimuths.